On Thin Ice: The Mechanics of Failure in Sea Ice

Dominic Vella

March 15, 2007

1 Introduction

Sheets of floating ice are rarely at rest or found in isolation. They are driven by wind and water stresses and hence collisions with other sheets are unavoidable. The focus of this report is on the mechanical aspects of slow collisions between thin sheets of floating ice. Such interactions underlie the mosaic of patterns found in the world's most extensive bodies of floating ice — sea ice — and hence are of geophysical importance. However, we are drawn to the topic by the simple fact that the patterns resulting from collisional interactions are visually arresting and may have mechanical implications that extend beyond the system that motivates our work. We begin with a description of some of the phenomenology that we aim to understand.

In sea ice, where the "sheets" of relevance are called "floes", collisions are observed to create three families of patterns. The creation of each family, which can be characterized by a post-collision pattern or morphology, can be envisioned either as the result of the compression of a single sheet, or floe, of ice that fails and forms two floes which continue to collide, or the collision between two pre-existing floes. Often, due to the inhomogeneities of the floes involved, or the forcing that drives them together, some combination of these three patterns is observed in the field.

The most destructive of these families of ice patterns is the pressure ridge in which the two ice floes break up as they collide thereby forming a "sail" and a "keel" of highly fractured ice blocks. Less destructive are the two types of rafting illustrated in figure 1: simple rafting and finger rafting. In simple rafting, one ice floe rides over the adjoining floe without the creation of a large amount of rubble. Finger rafting is similar to simple rafting in the sense that the two floes alternately ride over and under one another forming a series of interlocking fingers. Generically, these fingers have very sharp linear features that are particularly striking — as is the well-defined spacing of the fingers.

For those interested in geophysical scale modelling of the interaction of sea ice with the atmosphere and the ocean, these deformation processes are particularly important. For example, the ridging and rafting of ice alters the albedo of the ice cover significantly (in rafting, the ice doubles in thickness and so appears much whiter than surrounding ice) and plays a major role in the mechanical redistribution of sea ice thickness [2]. Rothrock [15] also provides reasons for studying these deformation phenomena:

Figure 1: Rafting of thin sea ice. Left: 'simple' rafting of one floe over another in the Beaufort Sea. Note the crack formation parallel to the free edge of the ice. Right: 'finger' rafting in the Amundsen Sea. Photographs courtesy of Wilford Weeks [21].

> "*If we knew what the constitutive equation for pack ice should be, we would not need to pay attention to the mechanisms of floe interaction. But the simple fact is that we are not at all sure about the constitutive equation . . . we have turned to the study of these mechanisms — rafting, ridging, shearing, and opening — to deduce what we can about the large-scale mechanical behavior of pack ice.*"

Because the families of deformation patterns are intrinsically interesting, our outlook on the value of this study is one of optimism. We would like to understand the formation of finger structures in finger rafting and determine what the characteristic width of the resulting fingers is. We would also like to characterize the precise conditions under which each of the three deformation patterns is observed.

2 Governing equations

Throughout this report, we shall model an ice floe as a thin elastic sheet floating on a denser liquid: water. In this section we describe the governing equations for a thin plate, including the effects of in-plane forces. Some detail on the origin of these equations is given by Mansfield [12].

The midplane displacement, $w(x, y)$, of a thin elastic plate subject to a pressure p is determined by a balance of forces on the plate. If we introduce a force function φ to ensure that forces are balanced in the plane of the plate, then the normal force balance leads to the governing partial differential equation

$$B\nabla^4 w = p + [w, \varphi] \tag{1}$$

where B is the bending stiffness, or flexural rigidity, of the plate and

$$[a, b] \equiv \frac{\partial^2 a}{\partial x^2}\frac{\partial^2 b}{\partial y^2} - 2\frac{\partial^2 a}{\partial x \partial y}\frac{\partial^2 b}{\partial x \partial y} + \frac{\partial^2 a}{\partial y^2}\frac{\partial^2 b}{\partial x^2}. \tag{2}$$

B is related to the plate thickness, h, as well as the elastic properties of the material (the Young's modulus, E, and Poisson ratio, ν) by

$$B = \frac{Eh^3}{12(1-\nu^2)}. \tag{3}$$

For an elastic sheet (of density ρ_s) floating on a liquid (of density ρ) the pressure p is simply the hydrostatic pressure in the liquid. With no forces other than gravity acting, the sheet will float with $w = w_\infty \equiv h(1/2 - \rho_s/\rho)$. For simplicity, therefore, we shall measure all vertical displacements relative to this equilibrium level. The pressure p is then given by $p = -\rho g w$ from which it immediately follows that

$$B\nabla^4 w + \rho g w = [w, \varphi]. \tag{4}$$

For a displacement (u, v, w), the in-plane strains, ϵ_{ij}, are given by

$$\epsilon_{xx} = u_{,x} + \tfrac{1}{2}w_{,x}^2, \quad \epsilon_{yy} = v_{,y} + \tfrac{1}{2}w_{,y}^2, \quad \epsilon_{xy} = \tfrac{1}{2}(u_{,y} + v_{,x} + w_{,x}w_{,y}), \tag{5}$$

where $w_{,x}$ denotes the partial derivative of w with respect to x and so on (hopefully avoiding confusion with the various components of tensors). The displacements u and v may be eliminated from these relationships using the condition of compatibility (e.g., [12], pg. 13). Relating the strains to the in-plane forces and hence to the derivatives of the force function φ, it is possible to show that

$$\nabla^4 \varphi = -\tfrac{1}{2}Eh[w, w]. \tag{6}$$

Equations (4) and (6) may be non-dimensionalized by rescaling lengths with $\ell_* \equiv (B/\rho g)^{1/4}$ and the force function φ with the bending stiffness. In this analysis, ℓ_*, the length scale over which vertical deflections of the floe decay, plays a central role. We use uppercase letters to denote dimensionless quantities so that $X = x/\ell_*$, $\Phi = \varphi/B$ and so on. Equations (4) and (6) may then be rewritten as

$$\nabla^4 W + W = [\Phi, W], \tag{7}$$

and

$$\nabla^4 \Phi = -\tfrac{1}{2}\mathcal{S}[W, W] \tag{8}$$

respectively. Equations (7) and (8) are commonly attributed to one or both of Föppl and von Kármán (e.g., [12]).

In (8) we have introduced the dimensionless stretching stiffness

$$\mathcal{S} \equiv \frac{Eh}{(B\rho g)^{1/2}}, \tag{9}$$

which measures the relative ease with which the ice floe stretches and bends to accommodate deformation. Note that because $B \sim h^3$, $\mathcal{S} \sim h^{-1/2}$, and hence for the thin ice floes that are of interest here, we expect to find that $\mathcal{S} \gg 1$ so that deformation can be accommodated more easily by bending than stretching. This expectation is vindicated by substituting some typical values for the material properties of ice, as is shown by the data collected in table 1. This table also gives typical values for the characteristic length ℓ_* based on these material properties.

	Material Properties			Values for $h = 0.1$ m		
Ice type	E (GPa)	ν	σ_m (MPa)	ℓ_* (m)	$\mathcal{S}$	Reference
Fresh	$0.3 - 12$	0.33	$1 - 3$	3.1 ± 0.1	10^4	[8, 17]
Sea	$0.1 - 0.9$	—	$0.1 - 0.4$	$1 - 1.7$	$1 - 3 \times 10^3$	[22]
Sea	1	0.29	0.4	1.75	3.4×10^3	[5]

Table 1: Typical values from the literature for the mechanical properties of ice. Here, σ_m is the yield strength, to be introduced later. Also shown are the implied values of the characteristic length ℓ_* and the non-dimensional stretching stiffness, $\mathcal{S}$.

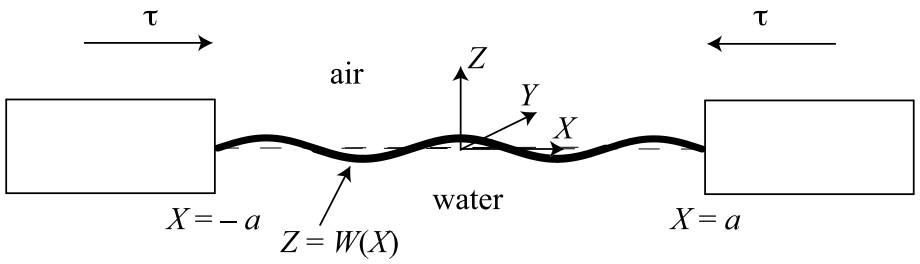

Figure 2: Schematic diagram showing a floating thin elastic sheet buckling under a compressive load τ.

3 The buckling failure of an ice floe

The most striking deformation patterns in sea ice are observed when two ice floes collide. This commonly occurs when a lead opens in thick ice and a thin layer of ice is formed by the freezing of ocean water in the lead. The movement of the thicker ice subjects the thin ice growing over the lead to large forces, which cause it to buckle and ultimately to fracture forming two or more floes. In this section we consider the buckling and subsequent failure of this thin ice.

In the two-dimensional buckling problem (illustrated in figure 2) there are no variations in the Y direction (i.e. into the page). The displacement of the ice plate, W, is therefore independent of Y and the Föppl -von Kármán equations (7)-(8) simplify to the system

$$W_{,4X} + W = \Phi_{,2Y} W_{,2X}, \quad \nabla^4 \Phi = 0. \tag{10}$$

Since $W = W(X)$, $\Phi_{,2Y} = f(X)$ and so $\Phi_{,XY} = A(X) + Y f'(X)$. However, $\Phi_{,XY}$ is just the traction exerted on the ice in the $Y-$direction, i.e. into the page. This traction is zero for compression purely in the $X-$direction and so we have $f'(X) = 0$ and $f(X)$ is a constant. Since the traction in the X direction is τ at the boundary $X = a$, we have $\Phi_{,2Y}(a) = -\tau$ and so $f(X) = -\tau$. Equation (10) therefore reduces to the ordinary differential equation

$$W_{,4X} + \tau W_{,2X} + W = 0. \tag{11}$$

The relevant boundary conditions to accompany (11) deserve some discussion. The thin layer of ice covering a lead is normally frozen into the thicker ice at the edge of the lead. We therefore take the boundaries of the thin ice at $X = \pm a$ to be clamped so that $W_{,X}(\pm a) =$

$W(\pm a) = 0$. The symmetry conditions about $X = 0$ suggest that a solution is the form $W(X) = A\cos kX$, where the wavenumber k satisfies

$$k^4 - \tau k^2 + 1 = 0. \tag{12}$$

There are, therefore, two possible wavenumbers, $k_\pm$, given by

$$k_\pm^2 = \tfrac{1}{2}\big(\tau \pm \sqrt{\tau^2 - 4}\big). \tag{13}$$

In general $W(X)$ will contain both of the wavenumbers given in (13). The condition of zero vertical displacement at $X = \pm a$ is satisfied by

$$W(X) = A\left(\frac{\cos k_+ X}{\cos k_+ a} - \frac{\cos k_- X}{\cos k_- a}\right), \tag{14}$$

where A is some (as yet undetermined) constant. The remaining boundary condition that $W_X(\pm a) = 0$ leads to a condition relating k_+ and k_-, namely the dispersion relation

$$k_+ \tan k_+ a = k_- \tan k_- a. \tag{15}$$

Since $k_\pm = k_\pm(\tau)$, the solutions of (15) determine the compressive force τ required to produce this displacement. For a given value of a, (15) has an infinite number of solutions, the smallest of which is $\tau = 2$. This corresponds to the smallest value of τ for which k_+ and k_- are real; it is shown in Appendix A that there are no solutions of (15) for complex $k_\pm$. When $\tau = 2$, $k_+ = k_-$ and (14) shows that $W \equiv 0$. Each value of $\tau > 2$ that solves (15) corresponds to a different mode of buckling in the ice floe. We shall consider only the lowest mode of buckling, which corresponds to the smallest value of $\tau > 2$ that solves (15).

Having determined τ by solving (15) the solution for the shape of the buckled ice floe is given by (14) up to the multiplicative constant A. The value of A is determined by the natural length, L, of the ice floe in its undeformed state. Neglecting any stretching of the ice floe and assuming small deformations, the contour length of the deformed floe must be equal to its natural length, i.e.

$$L = \int_{-a}^{a} \big(1 + W_{,X}^2\big)^{1/2}\, \mathrm{d}X \approx 2a + \tfrac{1}{2}\int_{-a}^{a} W_{,X}^2\, \mathrm{d}X. \tag{16}$$

In general, the ice floe may accommodate some of the imposed deformation by compressing (negative stretching). To account for this, we recall the expression for the strain ϵ_{XX} given in (5) and express the strain in terms of the force function Φ

$$U_{,X} + \tfrac{1}{2}W_{,X}^2 = \epsilon_{XX} = \frac{1}{\mathcal{S}}\big(\Phi_{,2Y} - \nu\Phi_{,2X}\big) = -\frac{\tau}{\mathcal{S}}. \tag{17}$$

Integrating this expression between $X = -a$ and a and using symmetry about $X = 0$, we find that

$$\int_0^a W_{,X}^2\, \mathrm{d}X = L - 2a\big(1 + \tau/\mathcal{S}\big). \tag{18}$$

Substituting the form of $W(X)$ from (14), we find that

$$\int_0^a W_{,X}^2\, \mathrm{d}X = A^2\left[\tfrac{a}{2}\big(k_+^2 + k_-^2\big) + ak_+^2\tan^2 k_+ a + k_+ \tan k_+ a\right], \tag{19}$$

which can be substituted into (18) to give A. Since k_+ and τ are determined by the numerical solution of (15), they depend only on the value of a. The shape of the ice floe can, therefore, be completely determined numerically for given values of a and L.

Beyond some critical compression, the stresses within the ice floe become so large that a crack is initiated within the ice and the ice fails, forming multiple floes. We now quantify this expectation using the results just obtained for the buckled shape of the floe. Throughout this report we shall assume that failure occurs when the maximum stress throughout the thickness of the ice floe reaches some critical failure stress, denoted by σ_m. For elastic plates, the stress varies linearly with the perpendicular distance, z, from the mid-plane. In particular, from [12] p. 5 we have

$$\sigma_{ij} = \frac{Ez}{(1-\nu^2)B} M_{ij}, \tag{20}$$

where M is the bending moment. The maximum stress is then achieved at the plate surface ($|z| = h/2$) and the ice will fail if

$$\sigma_m \leq \frac{Eh}{2(1-\nu^2)B} |M_{\max}| = \frac{6|M_{\max}|}{h^2}. \tag{21}$$

Implicit in the derivation of the failure criterion in (21) are two assumptions. The first is that ice behaves like a brittle material on the timescales of interest to us here. The second assumption is that strains vary linearly throughout the thickness of the floe. While these two assumptions are not always appropriate for floating ice, they are extremely convenient and are in good agreement with experiments to determine the maximum load that can be borne by an ice floe [9].

In the buckled state considered here,

$$|M_{\max}| = \frac{B}{\ell_*} \left|\left| W_{,XX} \right|\right|_\infty, \tag{22}$$

and so the ice will fail when

$$\left|\left| W_{,XX} \right|\right|_\infty = \frac{2\ell_*(1-\nu^2)}{h} \frac{\sigma_m}{E}. \tag{23}$$

Note that this relation suggests that for ice of given material properties, thin ice floes can support relatively large curvatures without breaking. By fixing L and calculating $\left|\left| W_{,XX} \right|\right|_\infty$ numerically for different degrees of compression, we find that typical ice floes fail while the ice deformation is small. In particular, figure 3 shows that the maximum slope of the interface is small at failure even for very thin ice floes. The linear theory presented here is, therefore, self-consistent and we may continue to make use of the linearized equations for the remainder of this report.

We note also from figure 3 that ice is very fragile and breaks readily under compression. To emphasize this point further, figure 4 shows the dimensional amplitude of the floe deflection at failure as a function of ice thickness. This shows that we can only expect to see very small amplitude buckles in unbroken ice. This is in accordance with the observation of Weeks [21] that it is very difficult to observe these buckles in the field unless there is drifting snow to highlight them.

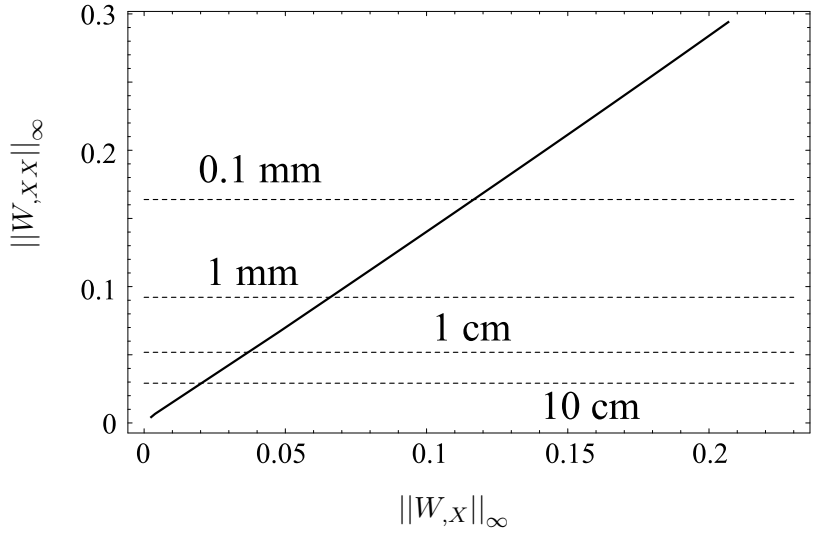

Figure 3: The magnitude of the maximum sheet curvature, $||W_{,XX}||_\infty$, as a function of the largest gradient of the buckling mode, $||W_{,X}||_\infty$. Here $\mathcal{S} = 10^3$, $L = 50$ and we have taken $\sigma_m = 2 \times 10^5$ Pa, $E = 3 \times 10^8$ Pa and $\nu = 0.3$ to plot horizontal dashed lines corresponding to the maximum curvature possible before failure for four different ice thicknesses.

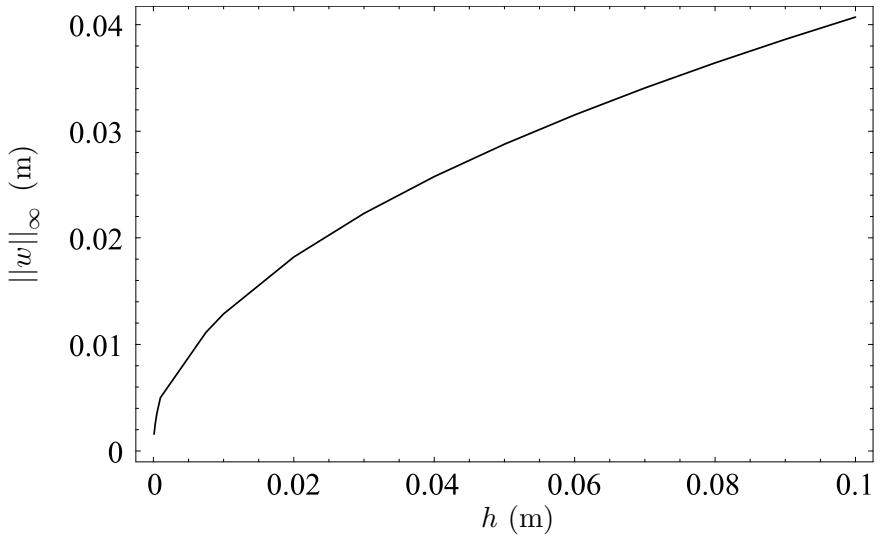

Figure 4: The maximum dimensional deflection of a buckled ice floe as a function of ice thickness, h. Here $\mathcal{S} = 10^3$, $L = 50$ and we have taken $\sigma_m = 2 \times 10^5$ Pa, $E = 3 \times 10^8$ Pa and $\nu = 0.3$ as typical values [14].

Figure 5: Photograph showing an end-on view of simple rafting. The overriding floe has failed in places, suggesting a close link between simple rafting and pressure ridging. Courtesy of John Wettlaufer.

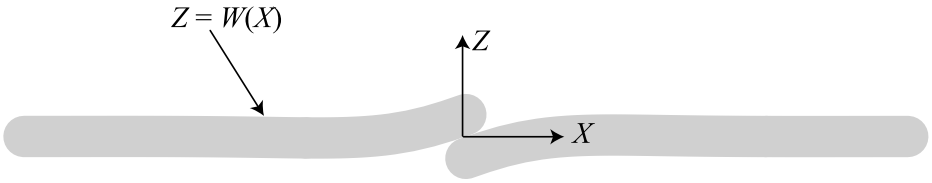

Figure 6: Schematic of two ice floes on the brink of rafting.

4 Rafting versus ridging

Having explored how a thin ice floe can buckle and then break under compression, we now move on to consider what happens once the ice has broken but the compression has not ceased. For simplicity, we shall consider two ice floes colliding, although the analysis in the previous section shows that two or more breaks may occur in general. Two outcomes of this collision seem plausible: either one ice floe may ride over the top of the other ('simple' rafting) or both ice floes may break as they come into contact causing an accumulation of rubble in a ridge. The photograph in figure 5 shows that these two possibilities are very closely related. Here, we show that there is a critical thickness above which ridging, rather than rafting, should occur. This is a result first derived by Parmerter [14], though we develop a much simplified model that leads to essentially the same result. This simplified analysis highlights the important physical principles that determine when rafting can occur.

Consider two ice floes in the configuration shown in figure 6 — the two floes are on the brink of rafting. In this scenario, any tension within the floes can only be balanced by friction in the very small overlapping region. We shall neglect this friction and hence neglect the tension within the floes. This means that the shape of each floe is governed by

(11) simplified by the assertion that $\tau = 0$, i.e.

$$W_{,4X} + W = 0. \tag{24}$$

Solving this equation subject to the jump in plate height at $X = 0$:

$$W(0^-) - W(0^+) = H \equiv h/\ell_*,$$

and the continuity of the first three derivatives of W at $X = 0$, we find that

$$W(X) = \begin{cases} \frac{H}{2}\exp(X/\sqrt{2})\cos(X/\sqrt{2}), & X < 0 \\ -\frac{H}{2}\exp(-X/\sqrt{2})\cos(X/\sqrt{2}), & X > 0. \end{cases} \tag{25}$$

From this expression, it is a simple matter to show that the maximum bending moment in the two plates occurs at $X = \pm\pi/2\sqrt{2}$ and has a value

$$|M_{\max}| = \frac{Bh}{\ell_*^2}\frac{\exp(-\pi/4)}{2\sqrt{2}}. \tag{26}$$

For rafting to be possible we require that this bending moment be less than the maximum allowed by the failure criterion (21). In dimensionless terms, we require that the thickness satisfy

$$H < H_c \equiv 2^{5/4}e^{\pi/8}(1-\nu^2)^{1/2}\left(\frac{\sigma_m}{E}\right)^{1/2} \tag{27}$$

for rafting to be possible. Note that dimensional analysis leads us to expect that $H_c = f(\sigma_m/E)$. The functional form of f cannot be determined without this detailed calculation, however. In dimensional terms, (27) reads

$$h < h_c = \tfrac{8}{3}e^{\pi/2}\frac{1-\nu^2}{\rho g}\frac{\sigma_m^2}{E}, \tag{28}$$

which has the same dependence on material properties as the result given by Parmerter [14] but with a prefactor ≈ 12.8 rather than 14.2. Our approach has the advantage of being analytic, rather than numerical, and arises from a much simpler model of the rafting process.

We can use the typical values given in table 1 for the material properties of ice to give an estimate for h_c. Because these properties are sensitive functions of temperature and salinity, we must be careful to use estimates of σ_m and E observed in the same sample — mixing values from a weak sample (small σ_m) with those of a stiff sample (large E) can confuse the issue. We find that 12 cm $\leq h_c \leq$ 19 cm, which brackets the transition thickness of 15 cm described in the context of field observations [24].

Above the critical thickness given in (28) we expect that the ice floes will break before rafting can occur and a pressure ridge will be formed. In particular, the maximum bending moment occurs a dimensional distance $\pi\ell_*/2\sqrt{2}$ away from the contact region and so we expect that a crack will form here and will be parallel to the edge of the floe. The simple rafting shown in figure 1 shows just such a crack forming. We expect also that the blocks within the resulting pressure ridge should have this typical size. Weeks and Kovacs [24]

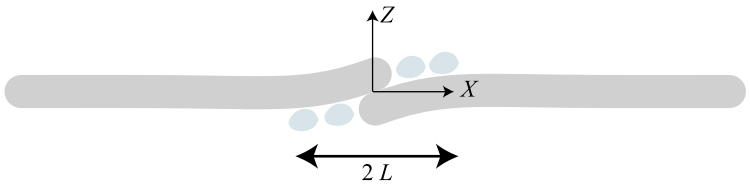

Figure 7: Schematic of two ice floes preloaded by rubble formed during failed rafting.

report that in one particular pressure ridge they found ice of thickness 30 cm and thickness/length ratio in the range $0.1-0.2$. This compares well with the calculated ratio, which should lie in the range $0.07-1.2$ based on the typical material properties of ice.

On occasion, ice has been reported to raft even though it was well above the critical thickness given in (28); rafting has been reported in ice up to 2 m thick. In these instances, it is also reported that the region where rafting occurs is covered with rubble formed by previously broken ice. Babko *et al.* [2] suggested that the presence of this rubble could lift one floe above the other, thereby facilitating rafting. In particular, consider two floes on the brink of rafting, as shown in figure 7. If these floes are too thick to raft in the configuration shown in figure 6, pieces will break off of them. The weight of overlying rubble formed from the overlying floe will depress the subducting floe further while the buoyancy of submerged ice blocks from the subducted floe will lift the overlying floe further. Here, we present a simple model to quantify how much of an effect this preloading could have and whether it can significantly alter the critical thickness at which rafting occurs.

We imagine that the region $-L < X < L$ is covered in rubble: this weighs down the ice floe with $X > 0$ and lifts the ice floe with $X < 0$. The shape of the two floes is obtained by solving (24) modified to incorporate the loading produced by the rubble. The appropriate boundary conditions are the same as in the earlier calculation leading to (25). This yields the floe displacement

$$W(X) = \begin{cases} \frac{H(1-r)}{2}\exp(\eta)\cos\eta + \frac{Hr}{2}\exp(\xi)\cos\xi, & X < -L \\ H(1-r) - \frac{H(1-r)}{2}\exp(-\eta)\cos\eta + \frac{Hr}{2}\exp(\xi)\cos\xi, & -L < X < 0 \\ -Hr - \frac{H(1-r)}{2}\exp(-\eta)\cos\eta + \frac{Hr}{2}\exp(\xi)\cos\xi, & 0 < X < L \\ -\frac{H(1-r)}{2}\exp(-\eta)\cos\eta - \frac{Hr}{2}\exp(-\xi)\cos\xi, & X > L, \end{cases} \tag{29}$$

where $r \equiv \rho_s/\rho$ is the non-dimensional density of the ice and

$$\xi \equiv \frac{X+L}{\sqrt{2}}, \quad \eta \equiv \frac{X-L}{\sqrt{2}}. \tag{30}$$

The maximum bending moment in either floe may then be determined numerically using the solution in (29) for given values of r and L. The results in figure 8 show the maximum curvature as a function of the extent of rubble, L, for three different values of the density ratio r. These curves show that as $L \to \infty$ the maximum curvature tends to a constant value. Considering the asymptotic limit $L \gg 1$, we find that the maximum value of $||W_{,XX}||_\infty$ occurs at $X \sim \pm\pi/2^{3/2} \pm L$ from which it immediately follows that the maximum curvature throughout the system is

$$||W_{,XX}||_\infty \sim \frac{Hr}{2\sqrt{2}}e^{-\pi/4}. \tag{31}$$

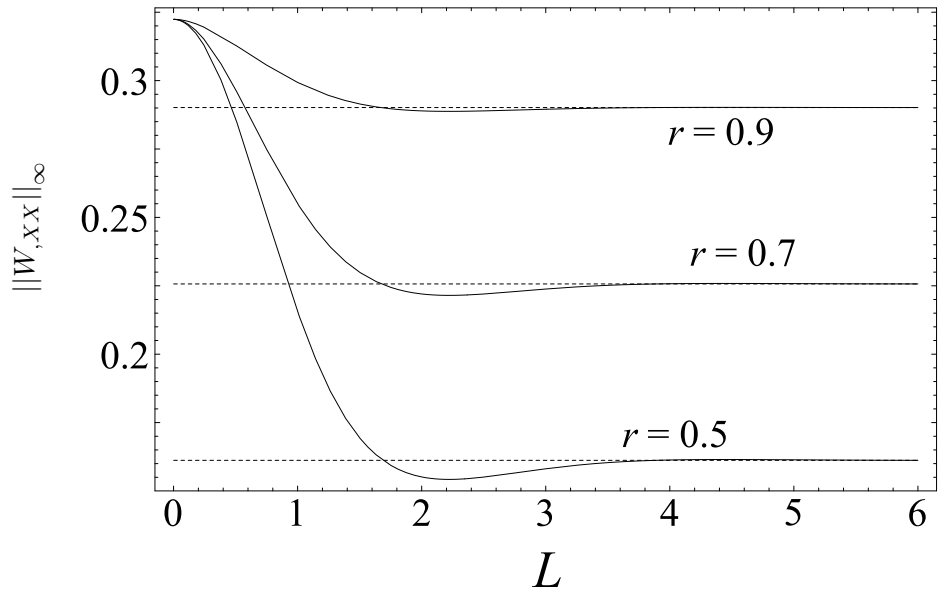

Figure 8: The maximum curvature in ice floes loaded/supported with rubble over a horizontal extent of L for three different values of $r = \rho_s/\rho$. The dashed lines show the asymptotic result (31), which is valid for $L \gg 1$.

Following the same procedure that led to (27), we find that the maximum non-dimensional thickness, H_c^*, for which rafting can occur is

$$H_c^* = \frac{2^{5/4} e^{\pi/8} (1-\nu^2)^{1/2}}{r^{1/2}} \left(\frac{\sigma_m}{E}\right)^{1/2}, \tag{32}$$

which is precisely the same result as presented in (27) modified by a factor $r^{-1/2}$, i.e. $H_c^* = r^{-1/2} H_c$.

For ice, $r \approx 0.9$ and so in dimensional terms this mechanism can account for an increase of about 25% in the maximum thickness for which rafting can occur ($h_c^* = r^{-2} h_c \approx 1.23 h_c$). It seems that this mechanism could explain rafting in slightly thicker ice (up to $h \approx 25$ cm, say) but does not explain rafting in much thicker ice. We therefore conclude that the large discrepancy must instead be attributed to variations in the mechanical properties of the ice, as well as the complex rheology and geometry [16] of sea ice. In this regard, note that the data presented by Weeks and Anderson [22] shows that σ_m is a very sensitive function of salinity while E is more sensitive to temperature.

5 Finger rafting

In the remainder of this report, we shall be concerned with understanding a more exotic form of rafting between two ice floes: the formation of interlocking fingers that ride over and under one another. This is commonly called finger rafting because of the striking finger patterns that form (see figure 1).

5.1 Field observations

Several authors have written about the phenomenology of finger rafting from their observations in the field. These include not only observations in sea ice (starting with Weeks and Anderson [23]) but also observations in fresh water ice by Weber [20] and Green [7]. Tuhkuri and Lensu [19] have also observed some evidence of finger rafting in their ice-tank experiments using a mixture of ethanol and water. With the exception of the field observations of Mahoney and others [11], all observations of finger rafting have been limited to very thin ice; typically $h < 10$ cm.

As well as being the thickest ice for which finger rafting has been reported, the wavelength of the fingering pattern observed by Mahoney is also large. Does the thickness of the ice influence the wavelength of the finger rafts that are formed? We have collated the reported estimates of ice thickness and the wavelength of the fingering pattern (reported and measured from published photographs). Table 2 shows this collection of data, and seems to suggest that the narrowest fingers occur in the thinnest ice. This correlation between ice thickness and wavelength was suggested by Green [7] although Weeks and Anderson [23] believed that there was no such correlation.

5.2 Finger rafting in wax

To the best of our knowledge, finger rafting has been reported only in ice floating on water. This might lead the reader to think that the appearance of fingers is reliant on some property of ice that is not common in solids. To investigate whether this is in fact the case, and hence determine the extent to which the phenomenon is of a general mechanical nature, we have conducted experiments using very thin layers of solid sealing wax floating on water to mimic ice floes. The sheets of wax were manufactured by pouring molten wax onto a solid substrate covered with a flexible film of polyvinylidene chloride (a.k.a. saran wrap). After the wax has cooled, the polyvinylidene chloride film may be peeled away leaving a thin wax sheet. It is difficult to ensure that the thickness is uniform, but this seems not to matter a great deal.

The mechanical properties of the same sealing wax were kindly characterized by Larry Wilen of Unilever using an ultrasonic apparatus. His experiments showed that for frequen-

Thickness	Wavelength	Ice type	Reference	Symbol
$2-3$ mm	$6-20$ cm	Fresh ice	[7]	■
$3-8$ mm	2 m	Fresh ice	[7]	■
$1-2$ cm	10 m	Fresh ice	[7]	■
$2-6$ cm	$2-8$ m	Sea ice	[23]	▲
$2.5-6.9$ cm	$4-6$ m	Ethanol–water	[19]	★
$3.5-4.5$ cm	$7-9$ m	Sea ice	[6]	◯
$1.3-1.5$ m	$20-100$ m	Sea ice	[11]	♦

Table 2: Field observations of ice thicknesses in which finger rafting has been reported and the wavelength of the resulting fingering pattern. The symbols indicated are used to plot these data in figure 11.

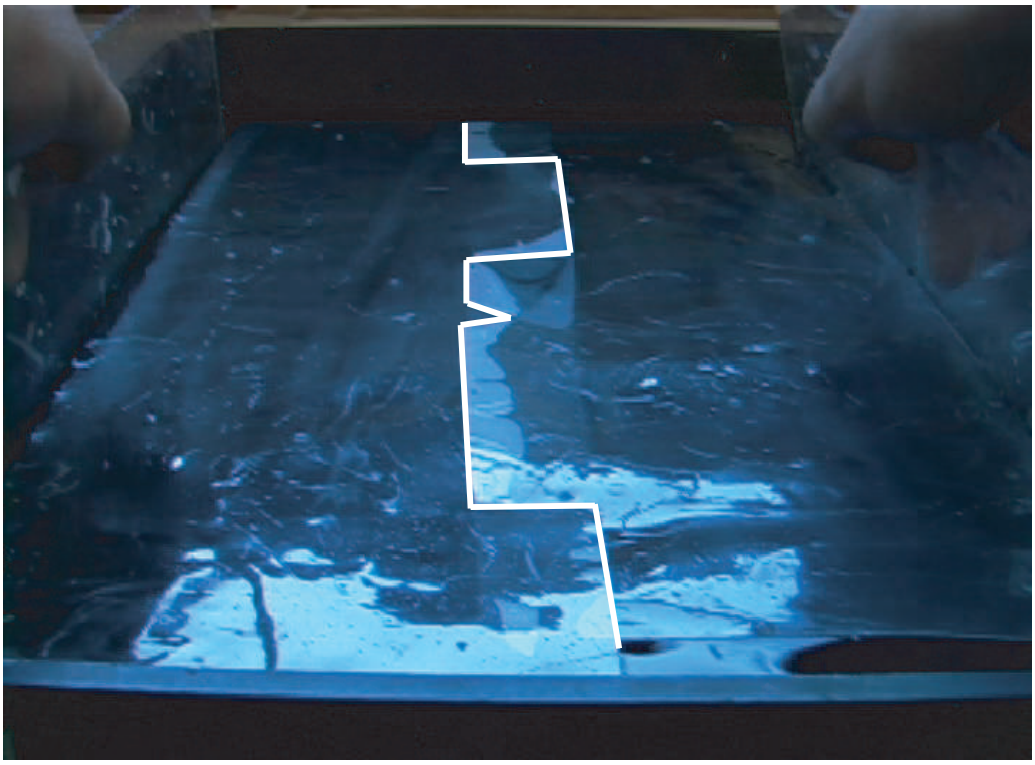

Figure 9: Experimental realization of finger rafting in thin wax sheets floating on water. Here the thickness of the wax sheets is in the range $150 - 500$ μm and the length of the sheets is around 40 cm. For clarity, the edge of the fingered wax sheets has been highlighted with a white line.

Figure 10: Plan view of finger rafting as observed in thin wax sheets of thickness in the range $170 - 380$ μm. The total field of view here is around 30 cm.

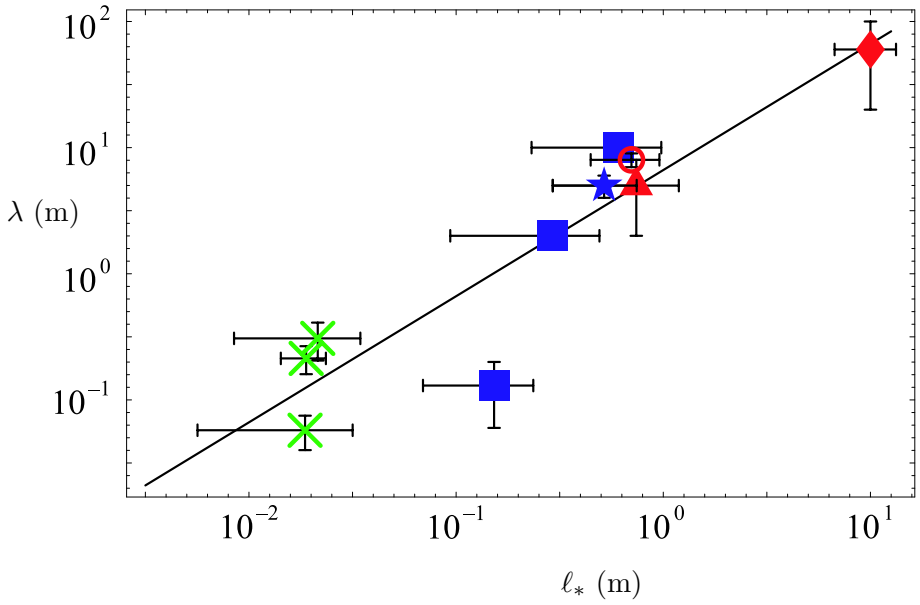

Figure 11: Wavelength of fingering pattern, λ, for floating sheets with differing characteristic lengthscales, ℓ_*. The data plotted here are a combination of those in table 2 (obtained from the field observations of others) and our own experiments with thin sheets of wax floating on water (denoted by $\times$). The colouring of points signifies the type of solid in which the finger rafting was observed — sea ice, fresh ice and sealing wax. The line shows the theoretical prediction (40).

cies in the range $10^{-2} - 10^2$ Hz the Young's modulus lies in the range $1.57 \times 10^8 - 1.16 \times 10^9$ Pa, assuming a Poisson ratio $\nu = 0.3$. These experiments also demonstrated a solid-solid phase transition in the wax at a temperature close to 35°C. Above this temperature the wax becomes ductile and does not fail under loading. Rather, it deforms plastically. We therefore ensured that the wax was allowed to cool to room temperature before performing the experiments reported here.

The thin wax sheets were floated on water with their long edges in contact and then pushed together by hand. As shown in figures 9 and 10, we observed finger rafting. Experimental constraints, the most important of which were the ability to accurately control the thickness of the wax and to avoid edge effects in the transverse direction, limited the number of fingers observed. However, the fingers shown in figures 9 and 10 have the strong rectilinear features reported of finger rafting ice. Moreover, plotting the typical wavelength of this fingering pattern (λ) as a function of the characteristic length ℓ_* seems to show reasonable collapse with field observations of finger rafting in ice, as shown in figure 11. Note that $\ell_* \sim h^{3/4}$ and so there is some correlation between λ and h.

5.3 A physical mechanism

Several authors have suggested that finger rafting occurs because of wave action [3, 4, 23]. Although their mechanisms differ in terms of details, the essential ingredients are the same

and may be paraphrased as follows. Finger rafting is initiated when a small portion of one ice floe is deposited on top of another ice floe by an advancing wave crest. This leaves a portion of the ice out of water and not supported by another ice floe. A tear forms in this area (since sea ice is not strong enough to support its own weight) and a first finger is formed. As the wave crest passes on, the other ice floe protrudes onto the first, tears and forms a finger pointing in the opposite direction to the first. As more waves are incident on the ice, a series of prototype interlocking fingers is formed which grow as the ice floes are compressed and the ice floes plough through one another.

While this explanation may be correct in many circumstances, it cannot form the basis of a general theory of finger rafting. Firstly, in nature finger rafting occurs when there is wind but no open water for the generation of a swell [7]. Secondly, the mechanism above relies on the fact that sea ice cannot support its own weight and so will fail if not supported by either water or other regions of ice. This is certainly not the case for the thin sheets of wax used in our laboratory experiments, and is also unlikely to be the case in the fresh water situations for which finger rafting has been observed.

An alternative explanation relies on some small overlap between the two ice floes (see figure 12): if a small portion of ice floe A overrides ice floe B at a point C, floe A is lifted slightly at the point C by the additional buoyancy provided by the presence of floe B. Conversely, floe B is depressed at the point C by the additional load provided by the presence of floe A. As we have seen many times already in this report, the characteristic response of an ice floe to such perturbations is not monotonic decay in the far field but rather an oscillatory deflection modulated by an exponential decay. We therefore expect that away from the point C both floes A and B will have an oscillatory vertical deflection, shown schematically in figure 12. In particular, the free edges of the two floes should have an oscillatory vertical deflection. Moreover, because the initial perturbations to each of the floes are of opposite sign, these oscillations remain out of phase along the length of the free edge: crests of floe A correspond to troughs of floe B and vice versa. The free edges of the two floes are displaced vertically relative to one another. Thus, these out of phase oscillations cause the two floes to form interlocking thrusts during subsequent compression.

Because the displacement of the floe decays exponentially away from the protrusion, we do not expect an overlap at one place to be sufficient for finger rafting everywhere; the vertical displacement must be a reasonable fraction of the thickness for the oscillations we describe to give rise to floes running over one another. Instead, we propose that the rafting propagates along the edge rather like a zipper: when rafting occurs in one place the displacements nearby are sufficient to cause finger rafting there too and so on. This wave of rafting should travel at the speed of gravity waves in water covered with an elastic sheet. The phase speed, c, of these waves [18] depends on their wavenumber, k, and is given by

$$c^2 = \frac{Bk^4 + \rho g}{\rho_s h k^2 + \rho k}. \tag{33}$$

In our wax experiments, the speed of the waves with wavenumber ℓ_*^{-1} is typically around 0.5 ms^{-1}, making this zippering unobservable within the scope of the technology we employed. For ice of thickness 10 cm, this wave speed is on the order of 5 ms^{-1}.

The mechanism we have described does not rely on any material properties that are peculiar to ice, though we do require the solid material to be able to tear to form fingers as

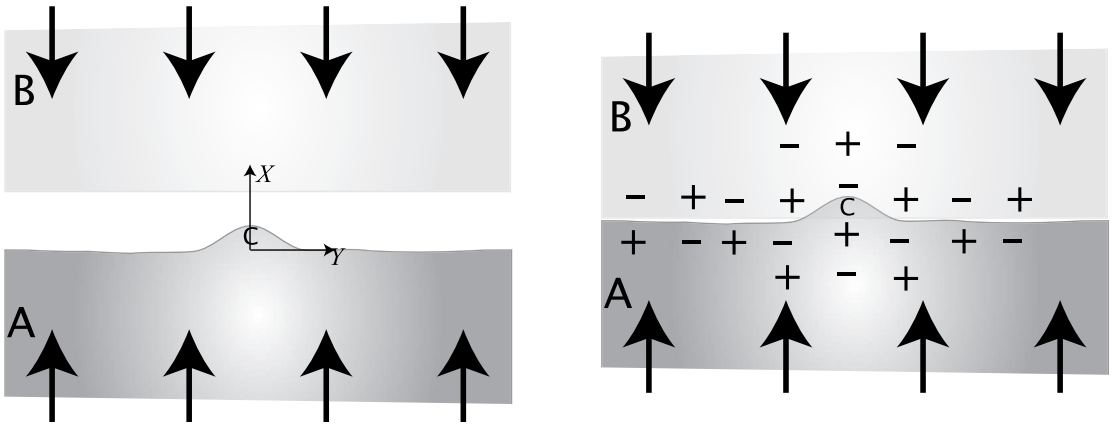

Figure 12: Plan view of two ice floes A and B colliding. A small protrusion in floes A leads to an overlap of the floes in a small region, C. This overlap causes oscillations in the vertical position of the floes, which decay away from C. The sign of these displacements is indicated by the $+/-$ symbols in the figure. Notice that the oscillations along the free edge are exactly out of phase in the two floes causing the two floes to alternately ride over and under each other under compression (arrows).

the two floe edges are pushed past one another. This condition seems also to be satisfied by wax whereas other materials, such as aluminium foil, do not tear sufficiently easily and so cannot form these fingers.

5.4 The deflection of a semi-infinite elastic plate

A mechanism resembling that presented above seems to have been outlined briefly by Fukutomi and Kusunoki [6]. They discuss finger rafting only cursorily and give a very vague presentation of a model of a point force acting on an infinite elastic sheet to give some idea of the scale of fingers formed. However, they give no details of their calculations nor of the equations solved. Here, we rectify this situation by presenting a thorough analysis of the problem.

We modify the earlier analysis of rafting to incorporate the effect of a vertical load, F, on a semi-infinite ice floe. Again neglecting the in-plane forces, we find that the deflection of the floe satisfies

$$\nabla^4 W + W = F(X, Y) \tag{34}$$

The Green's function for the deflection of an semi-infinite elastic plate on an elastic foundation was given by Kerr and Kwak [10] as well as Nevel [13]. Because an elastic foundation is exactly analogous mathematically to a floating sheet, we shall make extensive use of their result in what follows. In particular, if a concentrated force of dimensional magnitude f is applied at the point (X_0, Y_0), as shown schematically in figure 13, then the

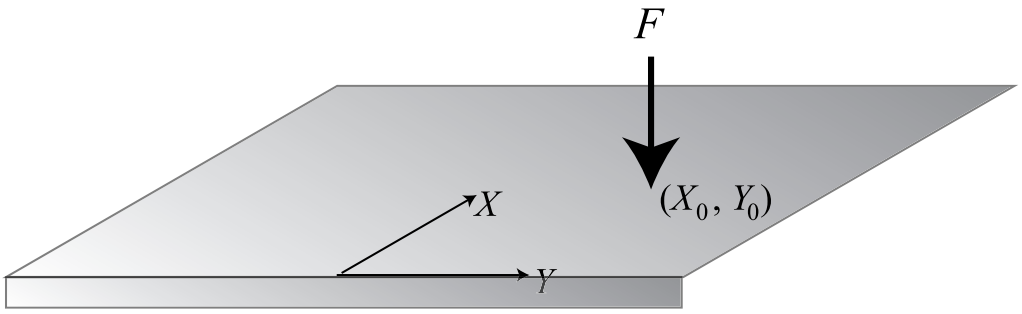

Figure 13: A point force F acting at the point (X_0, Y_0) on a semi-infinite floating elastic sheet.

vertical displacement at a point (X, Y) is given by

$$\pi\frac{\rho g\ell_*^3}{f}W(X,Y;X_0,Y_0) = -\tfrac{1}{2}\big[\mathrm{Kei}(R_0^-)+\mathrm{Kei}(R_0^+)\big]+\int_0^\infty A(X_0,\alpha)e^{-k_+X}\Bigg\{\cos k_-X - \frac{k_+\big[2k_-^2+(1-\nu)\alpha^2\big]}{k_-\big[2k_+^2-(1-\nu)\alpha^2\big]}\sin k_-X\Bigg\}\cos\alpha(Y-Y_0)\ \mathrm{d}\alpha. \quad (35)$$

Here Kei is the Kelvin function of zeroth order [1], $R_0^\pm$ is given by

$$R_0^\pm = \big[(X\pm X_0)^2+(Y-Y_0)^2\big]^{1/2}, \quad (36)$$

$k_\pm$ is given by

$$k_\pm = \Big(\tfrac{1}{2}\big[\sqrt{\alpha^4+1}\pm 1\big]\Big)^{1/2}, \quad (37)$$

and

$$A(X_0,\alpha) = \frac{\exp(-k_+X_0)}{\sqrt{\alpha^4+1}}\frac{2k_+^2-(1-\nu)\alpha^2}{4k_+^2\big[k_-^2+(1-\nu)\alpha^2\big]-(1-\nu)^2\alpha^4} \times \big[k_-(k_-^2+k_+^2+\nu\alpha^2)\cos k_-X_0 - k_+(k_-^2+k_+^2-\nu\alpha^2)\sin k_-X_0\big]. \quad (38)$$

This expression simplifies considerably if we look at the case of a point mass acting at the origin (i.e. $X_0 = Y_0 = 0$). In particular, the profile of the plate along the free edge ($X = 0$) takes the form

$$W(0,Y) = \frac{F}{\pi}\left(-\mathrm{Kei}(|Y|)+\int_0^\infty A(0,\alpha)\cos\alpha Y\ \mathrm{d}\alpha\right), \quad (39)$$

where $F \equiv f/\rho g\ell_*^3$. This function can be plotted numerically but what is of most interest here is the position of the zeros of $W(0,Y)$, since these determine the regions in which the two ice floes can most easily ride over one another. The smallest Y_* satisfying $W(0,Y_*) = 0$ is $Y_* \approx 4.507$ with the next root occurring at $Y_* \approx 7.827$. Since the vertical displacement decays exponentially with increasing Y, we take the distance between these first two roots to be that determining the wavelength of the finger rafting pattern with the position of

subsequent fingers determined once the initial fingers are in place. We therefore expect that

$$\lambda \approx 2(7.827 - 4.507)\ell_* = 6.64\ell_*, \tag{40}$$

which agrees well with the results presented in figure 11.

While the case of a point mass acting on an elastic sheet is a convenient abstraction, our actual interest lies in determining how an ice floe responds to having a finger from another ice floe pressed on top of it. We therefore consider a finger of width $2a$ protruding a distance $2b$ onto another ice floe. Each infinitesimal element of the protruding finger contributes to the displacement of the overridden floe. Since the equation governing the displacement of the ice is linear, we can sum these displacements to give the displacement field due to the presence of the finger. An element of width δY_0 and length δX_0 has a weight $f = -\rho_s g h \ell_*^2 \delta X_0 \delta Y_0$. Summing the displacement due to all of these elements, we find that

$$\begin{aligned} W(X,Y) &= \int_0^{2b}\int_{-a}^{a} W(X,Y;X_0,Y_0)\ \mathrm{d}Y_0\ \mathrm{d}X_0 \\ &\equiv \frac{\rho_s}{\rho}\frac{h}{\ell_*}\omega(a,b,X,Y). \end{aligned} \tag{41}$$

We are particularly interested in determining whether we need a large perturbation to initiate finger rafting. For the mechanism of finger rafting proposed here to be reasonable, we need the edge displacement induced by the overlap to be comparable to the ice thickness near the position where the load is being applied. To investigate whether this is the case, we calculated the rescaled displacement at the origin, $\omega(a,b,0,0)$, as a function of finger size for a square finger (i.e. $a = b$). Because of the definition of ω, the displacement becomes of the same order as the thickness when $\omega = \mathcal{O}(1)$.

The numerically determined dependence of ω on a is shown in figure 14. These results show that as a finger gets larger the vertical displacement at the origin grows quickly. Indeed, upon expanding the integrals in the definition of ω for $a, b \ll 1$, we find that

$$\omega(a,b,0,0) \sim \frac{4ab}{\pi}\left[\int_0^{\infty} A(0,\alpha)\ \mathrm{d}\alpha - \mathrm{Kei}(0)\right] \approx 1.848ab, \tag{42}$$

which agrees with the numerically computed values shown in figure 14 when $b = a \ll 1$. This asymptotic result is useful because it shows that the displacement grows quadratically as the finger size increases — this ensures that increasing the size of the perturbation makes a large difference to the displacement field, since the size of the force applied by the finger increases greatly. In particular, the displacement does become $\mathcal{O}(1)$ even for relatively small finger sizes (i.e., values of a).

We also note that for $a \gg 1$, $\omega(a,a,0,0) \sim 1$. This is to be expected since in the limit that an ice floe is overlain by another floe, it must sink a vertical distance $\rho_s h/\rho\ell_*$ to increase its Archimedes buoyancy enough to balance the overlying weight.

5.5 A threshold thickness

Just as there was a critical thickness above which simple rafting is not possible, we expect that there might also be a critical ice thickness above which simple rafting, rather than

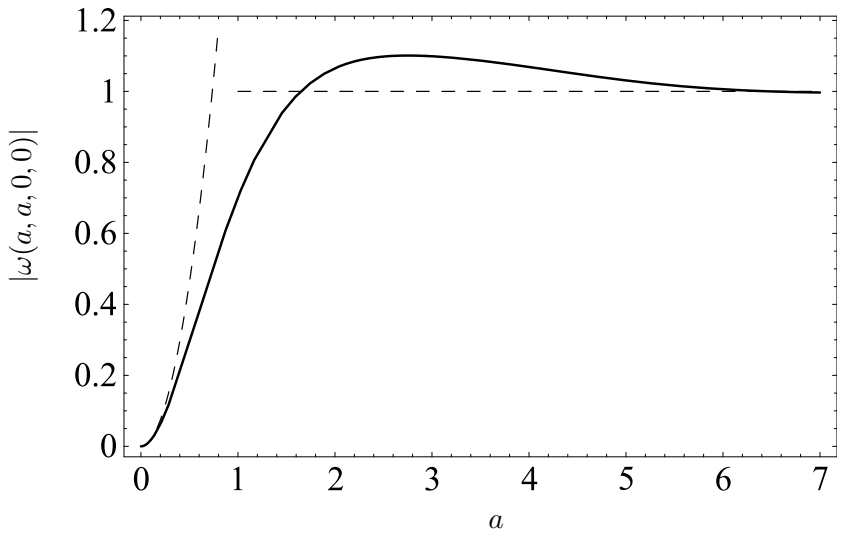

Figure 14: Plot of $\omega(a, a, 0, 0)$ for various values of finger size a (solid line). The dashed lines indicate the asymptotic expression (42) valid in the limit $a \ll 1$ and the limit $\omega \sim 1$ valid for $a \gg 1$.

finger rafting, will take place. Based on intuition gleaned from many field observations Weeks [21] suggests that for ice thicker than around 10 cm, finger rafting becomes rarer, presumably resulting instead in simple rafting.

As we found with the rafting/ridging transition discussed earlier, we expect that the generation of large moments within the ice may cause the stresses within the ice to exceed the maximum value that the ice can support, σ_m. For simplicity, we will consider the moments generated in a plate when a rectangular finger of width $2a$ and length $2b$ from another floe sits above it. (The finger is imagined to occupy the region $0 \le X \le 2b$, $|Y| \le a$.) Explicit formulae for the moments generated by a point force are given by Kerr and Kwak [10], but are not reproduced here. After integrating these expressions over the square $0 \le X_0 \le 2b$, $|Y_0| \le a$ (as for displacements in the last section), the moments in the X and Y directions may be written

$$M_{xx}(X,Y) = -\frac{B}{\ell_*}(W_{,XX} + \nu W_{,YY}) \equiv \frac{\rho_s}{\rho}\frac{Bh}{\ell_*^2}\mu_x(a,b,X,Y)$$
$$M_{yy}(X,Y) = -\frac{B}{\ell_*}(\nu W_{,XX} + W_{,YY}) \equiv \frac{\rho_s}{\rho}\frac{Bh}{\ell_*^2}\mu_y(a,b,X,Y),$$

respectively.

The functions μ_x and μ_y may be evaluated by numerical quadrature. Our numerical results are in perfect agreement with those tabulated by Nevel [13], over his limited range of values of a and b. We find that the largest moments generated are in $\mu_y(a, b, 0, 0)$ so that the failure of the ice floe should be manifested in a crack perpendicular to the floe edge. This is contrary to the failure of simple rafting in which a crack formed parallel to the free edge of the ice floe.

To find a critical thickness above which finger rafting can no longer occur, we look

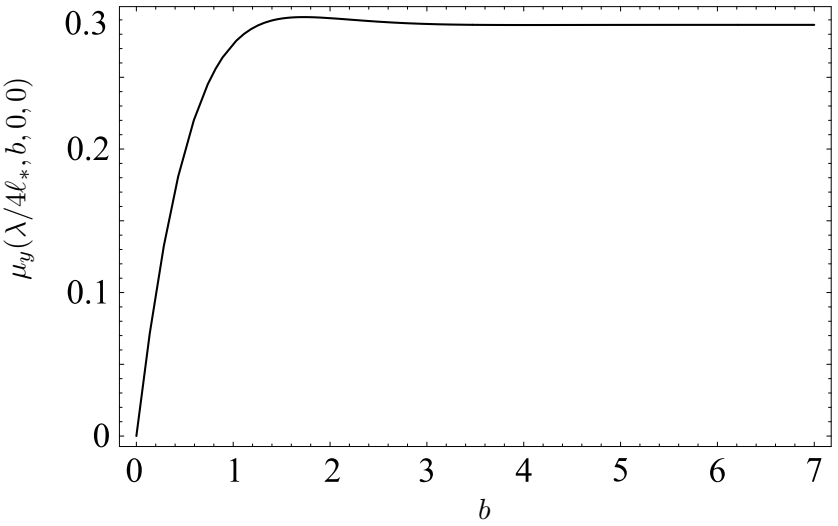

Figure 15: Plot of $\mu_y(\lambda/4\ell_*, b, 0, 0)$ as a function of the finger length b.

for the maximum value, μ_∞, of $\mu_y(a, b, 0, 0)$. Since we expect individual fingers to have a dimensional width of $\lambda/2$, where λ is given by (40), we choose $a = \lambda/4\ell_*$ and calculate $\mu_y(a, b, 0, 0)$ for this value of a.

Figure 15 shows the numerically computed values of $\mu_y(\lambda/4\ell_*, b, 0, 0)$. This demonstrates that there is indeed a maximum value, $\mu_\infty \approx 0.292$. Given this maximum moment we require that

$$\sigma_m > \frac{6}{h^2}\frac{\rho_s}{\rho}\frac{Bh}{\ell_*^2}\mu_\infty, \tag{43}$$

for the finger to be able to grow indefinitely without the ice beneath it breaking. This condition is satisfied provided that

$$H < \left[\frac{\rho}{\rho_s}\frac{2(1-\nu^2)}{\mu_\infty}\right]^{1/2}\left(\frac{\sigma_m}{E}\right)^{1/2} \approx 2.6\left(\frac{\sigma_m}{E}\right)^{1/2}. \tag{44}$$

The critical thickness at which finger rafting cannot happen scales with σ_m/E in precisely the same way as the critical thickness at which simple rafting gives way to ridging. However, the prefactor is different (and smaller!) suggesting that for a given value of σ_m/E we may be able to transition between finger rafting, simple rafting and ridging just be varying the ice thickness. The condition in (44) may be recast in dimensional terms as

$$h < \frac{\rho}{\rho_s}\frac{1-\nu^2}{3\rho_s g\mu_\infty^2}\frac{\sigma_m^2}{E}. \tag{45}$$

Taking typical values for the material properties of sea ice, we find that this transition thickness lies in the interval

$$4 \text{ cm} \leq h \leq 8 \text{ cm}. \tag{46}$$

This estimate is in reasonable agreement with the suggestion of Weeks [21] for a transition thickness on the order of 10 cm and is consistent with most of the field observations collected

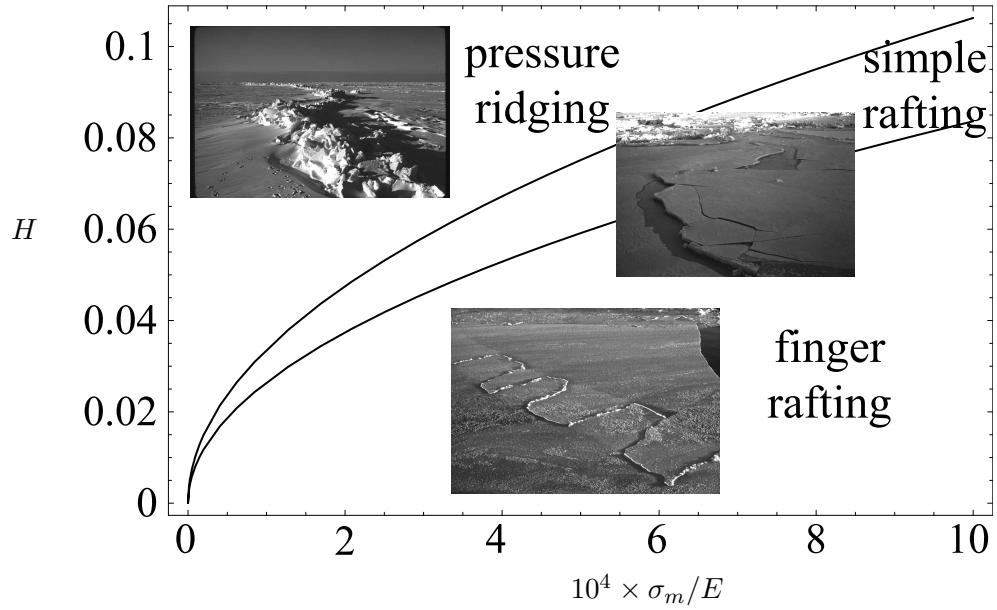

Figure 16: Regime diagram showing the values of σ_m/E and H for which we expect to observe each of the deformation types observed. Photographs courtesy of Wilford Weeks [21].

in table 2, for which finger rafting is observed in ice of thickness up to around 6 cm. This also provides some quantitative support for the statement of Weeks and Kovacs [24] that:

> "*Although less striking when observed from the air, simple rafting of thin ice... is actually more common than finger rafting.*"

Because the maximum bending moment in the floe is $\mu_y(a, b, 0, 0)$, we expect that a crack will form perpendicular to its edge. Perhaps this means that the finger breaks through the floe and is subducted beneath along with the remainder of the raft in simple rafting? We expect that above the critical thickness a finger might start to grow but will fall through the underlying ice once it reached a length of at most $4\ell_*$. However, we are unaware of observations wherein finger rafting metamorphoses into simple rafting against which to check this picture.

6 Conclusions

We have studied the mechanics of ice floe failure using ideas from thin plate theory. Because ice is so weak ($\sigma_m/E \ll 1$), thin plate theory allows us to study the buckling instability of an ice floe compressed by the motion of much thicker flanking floes up to the point at which the ice fails. We then focused on the three main types of deformation that result from the subsequent collision of two floes. By considering the forces induced by these different deformations we determined quantitative conditions on the different ice thicknesses for which each of these deformation patterns is observed. In particular, by plotting the dimensionless conditions (27) and (44) on the same graph, we obtain a regime diagram showing the

values of σ_m/E and H for which finger rafting, simple rafting and pressure ridging should be observed. Such a regime diagram is shown in figure 16. Although our main interest lies in the applicability of these results to floating ice, our experiments with wax sheets demonstrate that finger rafting may also be observed in systems other than ice. However, we do not expect the regime diagram shown in figure 16 to be quantitatively valid for other materials: ice typically has $\sigma_m/E < 10^{-3}$ so that the transitions between different regimes always have $H \ll 1$, and thus thin plate theory is valid. This is not generally the case for other materials.

Appendix A: The wavenumber in buckling is real

In section 3 we assumed that the wavenumber k observed in buckling is purely real so that there are no exponentially decaying modes. Here, we prove this assertion by supposing instead that there is a complex pair of wavenumbers $k_\pm$ satisfying (12). Since the tension τ is real, $k_\pm$ must be complex conjugates of one another and we may write $k_\pm = k_r \pm \mathrm{i}k_i$. The dispersion relation (15) then reads

$$(k_r + \mathrm{i}k_i)\tan(k_r + \mathrm{i}k_i)a = (k_r - \mathrm{i}k_i)\tan(k_r - \mathrm{i}k_i)a. \tag{47}$$

Expanding this equation and equating imaginary parts gives

$$f(ak_i) \equiv \frac{ak_i \cos^2 ak_i}{\cosh^2 ak_i} = -\frac{ak_r}{\tanh ak_r} \equiv g(ak_r). \tag{48}$$

A plot of the functions f and g reveals that their ranges do not overlap and so there cannot be any solution of (48) — our assumption that k was imaginary is incorrect and we have shown that k is, in fact, real.

Acknowledgments My experiments in wax would not have been possible without Keith Bradley's tolerance of my burning wax in the lab, the use of Neil Balmforth's camcorder, Lary Wilen's careful measurements of the Young's modulus of sealing wax and Rachel's impromptu (and uncalled for) karaoke sessions. I am grateful to Marcus Roper, L. Mahadevan and Neil Balmforth for discussions about the theoretical side of this work. Two people deserve special thanks. Firstly, Wilford Weeks has been incredibly forthcoming with all of the information that he has on these phenomena; he provided photographs from his upcoming book, his own translation of the Fukutomi and Kusunoki paper and has replied to what must seem like a deluge of emails. Secondly, for introducing me to this topic, helping in the lab, numerous conversations and maintaining his enthusiasm throughout the summer, cheers jsw!

References

[1] M. Abramowitz and I. A. Stegun, *Handbook of Mathematical Functions with Formulas, Graphs, and Mathematical Tables*, Dover, New York, 1964.

[2] O. Babko, D. A. Rothrock, and G. A. Maykut, *Role of rafting in the mechanical redistribution of sea ice*, J. Geophys. Res., 107 (2002). doi: 10.1029/1999JC000190.

[3] M. Dunbar, *Thrust structures in young sea ice*, J. Glaciol., 3 (1960), pp. 724–732.

[4] ——, *Note on the formation process of thrust structures in young sea ice*, J. Glaciol., 4 (1962), pp. 147–150.

[5] R. J. Evans and N. Untersteiner, *Thermal cracks in floating ice sheets*, J. Geophys. Res., 76 (1971), pp. 694–703.

[6] T. Fukutomi and K. Kusunoki, *On the form and formation of hummocky ice ranges*, Low. Temp. Sci., 8 (1951), pp. 59–88. In Japanese (free translation by S. Takagi and W. F. Weeks).

[7] J. C. Green, *Finger-rafting in fresh-water ice: Observations in Lake Superior*, J. Glaciol., 9 (1970), pp. 401–404.

[8] P. V. Hobbs, *Ice Physics*, Oxford University Press, 1974.

[9] A. D. Kerr, *The bearing capacity of floating ice plates subjected to static or quasi-static loads*, J. Glaciol., 17 (1976), pp. 229–268.

[10] A. D. Kerr and S. S. Kwak, *The semi-infinite plate on a winkler base, free along the edge, and subjected to a vertical force*, Arch. Appl. Mech., 63 (1993), pp. 210–218.

[11] A. Mahoney, H. Eicken, L. Shapiro, and T. C. Grenfell, *Ice motion and driving forces during a spring ice shove on the Alaskan Chukchi coast*, J. Glaciol., 50 (2004), pp. 195–207.

[12] E. H. Mansfield, *The Bending and Stretching of Plates*, Cambridge University Press, 1989.

[13] D. E. Nevel, *A semi-infinite plate on an elastic foundation*, Tech. Rep. 136, Cold Regions Research and Engineering Laboratory, 1965.

[14] R. R. Parmerter, *A model of simple rafting in sea ice*, J. Geophys. Res., 80 (1975), pp. 1948–1952.

[15] D. A. Rothrock, *The mechanical behaviour of pack ice*, Annu. Rev. Earth Planet. Sci., 3 (1975), pp. 317–342.

[16] D. A. Rothrock and A. S. Thorndike, *Measuring the sea ice-floe size distribution*, J. Geophys. Res., 89 (1984), pp. 6477–6486.

[17] E. M. Schulson, *The structure and mechanical behaviour of ice*, JOM, 51 (1999), pp. 21–27.

[18] V. A. Squire, W. H. Robinson, P. J. Langhorne, and T. G. Haskell, *Vehicles and aircraft on floating ice*, Nature, 333 (1988), pp. 159–161.

[19] J. Tuhkuri and M. Lensu, *Laboratory tests on ridging and rafting of ice sheets*, J. Geophys. Res., 107 (2002), p. 3125.

[20] J. N. Weber, *Ice thrust structures*, J. Glaciol., 3 (1958), p. 291.

[21] W. F. Weeks, *On Sea Ice*, University of Alaska Fairbanks Press, 2006. In Preparation.

[22] W. F. Weeks and D. L. Anderson, *An experimental study of strength of young sea ice*, Trans. Am. Geophys. Un., 39 (1958), pp. 641–647.

[23] ——, *Sea ice thrust structures*, J. Glaciol., 3 (1958), pp. 173–175.

[24] W. F. Weeks and A. Kovacs, *On pressure ridges*, Tech. Rep. IR505, Cold Regions Research and Engineering Laboratory, 1970.